Revision 1

(Word count: 8026)

Micropores and mass transfer in the formation of myrmekites

Takashi Yuguchi[a,*], Haruka Yuasa[a], Yuya Izumino[a], Kazuo Nakashima[a], Eiji Sasao[b], Tadao Nishiyama[c]

[a] Faculty of Science, Yamagata University, 1-4-12 Kojirakawa, Yamagata 990-8560, Japan

[b] Japan Atomic Energy Agency, 959-31, Jorinji, Izumi, Toki, Gifu 509-5102, Japan

[c] Faculty of Advanced Science and Technology, Kumamoto University, 2-39-1, Kurokami, Chuo-ku, Kumamoto 860-8555, Japan

* Corresponding author: T. Yuguchi/Orcid 0000-0002-6541-1615

E-mail address: takashi_yuguchi@sci.kj.yamagata-u.ac.jp

Tel: +81 23 628 4641/Fax: +81 23 628 4661

This is the peer-reviewed, final accepted version for American Mineralogist, published by the Mineralogical Society of America.
The published version is subject to change. Cite as Authors (Year) Title. American Mineralogist, in press.
DOI: https://doi.org/10.2138/am-2021-7956. http://www.minsocam.org/

ABSTRACT

The formation process of myrmekites in granitic rocks can help us to understand the mass transfer between minerals and hydrothermal fluids during the deuteric stage. The Toki granite, central Japan, has three types of myrmekites. Type A myrmekite is defined as a single layer. Type B myrmekite shows a composite texture consisting of two layers, namely, a myrmekite layer and an albite (Ab)-rich layer that is free of vermicular quartz. Type C has a composite texture with the following three layers: two myrmekite layers separated by one Ab-rich layer. Micropores are found in these myrmekites in the undeformed granite, which enable quantitative determinations of the volume decrease during myrmekite formation by measurement of the area of micropores. The areal relationship between the micropores and vermicular quartz in the myrmekites exhibited a high correlation (R^2 = 0.8352), thus indicating that the genesis of the micropores is evidently related to myrmekite formation. We derived the reaction equations for myrmekite formation based on the singular value decomposition method. The matrices for singular value decomposition involve the following volume factors: volume change during the reaction and volume ratios of the product minerals. The singular value decomposition indicates that the myrmekites are produced through the consumption of plagioclase and K-feldspar with an inflow of H_4SiO_4, Na^+, and H^+ from the hydrothermal fluid, accompanied by an outflow of Al^{3+}, Ca^{2+}, and K^+ into the fluid, which constitute essential mass transfers during myrmekite formation. The difference of pH in the hydrothermal fluid and inflow amounts of H_4SiO_4 and Na^+ can explain the reason why micropores occur in the myrmekites but not in the Ab-rich rim (layer); the smaller inflow of H_4SiO_4 and Na^+ from the hydrothermal fluid with lower pH

conditions yielded micropore production during myrmekitization, and the larger inflow of H_4SiO_4 and Na^+ from the hydrothermal fluid with higher pH conditions yielded the formation of the Ab-rich rim (layer) with few micropores. The sequential variations in the chemical characteristics of the hydrothermal fluid during the sub-solidus conditions were characterized by a gradual decrease in H_4SiO_4 (Si^{4+}), Fe^{2+}, Mn^{2+}, Mg^{2+}, and Na^+ and a gradual increase in Ca^{2+}, K^+, H^+, and F^-.

Keywords: myrmekite; micropore; mass transfer; image analysis; Toki granitic pluton

INTRODUCTION

Sub-solidus reaction textures such as coronas, kelyphite, and reaction zones have potential importance as a record of the pressure–temperature conditions (e.g., Joanny et al., 1991), and also as a source of information concerning diffusion and reaction kinetics (e.g., Fisher, 1978). In an undeformed granitic rock, myrmekites are produced by a sub-solidus reaction in the presence of hydrothermal fluids (Yuguchi and Nishiyama, 2007; Abart et al., 2014). The myrmekite has a symplectic intergrowth texture consisting of vermicular quartz and albite-rich plagioclase, which typically develops between K-feldspar and plagioclase (Phillips, 1974). Investigations of the mechanism of myrmekite formation in granitic rocks are important for understanding the mass transfer between minerals and hydrothermal fluids in the deuteric stage (e.g., Yuguchi and Nishiyama, 2008). This study deals with the mechanism of myrmekite formation in a granitic system, in which the Toki granitic body was used as a case study.

Previous studies have described the formation mechanisms and growth processes of myrmekites in deformed and undeformed granitic systems (e.g., Abart et al., 2014; Cisneros-Lazaro et al., 2019). In early research, the following six theories became dominant in the early discussions on the formation mechanism of myrmekites (Phillips, 1974): (1) simultaneous or direct crystallization (e.g., Spencer, 1938), (2) replacement of K-feldspar by plagioclase (e.g., Becke, 1908), (3) replacement of plagioclase by K-feldspar (e.g., Drescher-Kaden, 1948), (4) solid state exsolution (e.g., Schwanke, 1909), (5) incorporation of recrystallizing quartz in growing albite exsolved from K-feldspar (e.g., Shelley, 1964), and (6) miscellaneous hypotheses including combinations of some of the above hypotheses

This is the peer-reviewed, final accepted version for American Mineralogist, published by the Mineralogical Society of America.
The published version is subject to change. Cite as Authors (Year) Title. American Mineralogist, in press.
DOI: https://doi.org/10.2138/am-2021-7956. http://www.minsocam.org/

71 (e.g., Ashworth, 1972). The recent discussions pertaining to the mechanism of myrmekite
72 formation focuses on the volume relation from reactants to products, which were derived
73 from the "volume–composition relationship" by Gresens (1967). In examples of the use of
74 this approach, Menegon et al. (2006) and Abart et al. (2014) suggested that the replacement
75 is metasomatic on the scale of the myrmekite domains requiring addition of sodium and
76 calcium and removal of potassium from the reaction site, whereas silica and aluminium
77 were conserved across the reaction front. Yuguchi and Nishiyama (2008) constructed the
78 reaction equation for the formation of myrmekites, which was derived based on the
79 following two constraints: (1) the assumption of conservation of the solid volume with
80 arbitrarily specified closure components and (2) the assumption of closure of Al_2O_3
81 together with an arbitrarily specified volume factor. As a result, the formation of myrmekite
82 can be characterized by the decomposition and partial albitization of both K-feldspar and
83 plagioclase, triggered by the introduction of silicon and sodium into the boundary between
84 the feldspars (Yuguchi and Nishiyama, 2008).

85 The replacement of calcic/intermediate feldspar by albite, i.e., albitization, were
86 frequently associated with micropores during the hydrothermal alteration in plagioclase
87 (e.g., Hövelmann et al., 2010; Yuguchi et al., 2019). Although Menegon et al. (2006) first
88 described the microporosity within myrmekite in the deformed Gran Paradiso metagranite,
89 previous studies have not described the presence of micropores within myrmekites in
90 undeformed granites. Here, the occurrence of micropores in myrmekites is newly found in
91 the undeformed Toki granite and described in this study (see the Petrography section), and
92 this is indicative of a volume decrease from the reactant (magmatic plagioclase) to product

This is the peer-reviewed, final accepted version for American Mineralogist, published by the Mineralogical Society of America.
The published version is subject to change. Cite as Authors (Year) Title. American Mineralogist, in press.
DOI: https://doi.org/10.2138/am-2021-7956. http://www.minsocam.org/

(myrmekite). Therefore, the determination of the micropore volume is essential for solving the mechanism of myrmekite formation. Notably, previous studies constructed reaction equations of myrmekite formation on the assumption of a volume factor based on the volume–composition relationship (e.g., Abart et al., 2014) without observations of micropores. The morphology of micropores in myrmekites of the Toki granite is preserved because of the little deformation in the granite. In the undeformed granite, the image analyses for backscattered electron (BSE) images allowed us to determine quantitatively the area of micropores. The volume of the micropores was estimated from their area by simply assuming the area–volume equivalence. Therefore, the data enabled us to build the "quantitative volume decrease based on micropore analysis" into the reaction equation of myrmekite formation, which can be used to study probable mass transfer relations between minerals and hydrothermal fluids. An albite-rich layer of plagioclase with no vermicular quartz has developed within the myrmekites (seen the Petrography section). Composite textures transitional from the albite-rich layer to the myrmekite layer (or from the myrmekite layer to the albite-rich layer) are occasionally observed in the Toki granite. We examined the mass transfer leading to the formation of such composite myrmekites and the predominant factors involved in the formation of single myrmekites and composite myrmekites.

Biotite chloritization and plagioclase alteration occurred at temperatures between 180 and 350 °C, and the associated mass transfer between reactant minerals and hydrothermal fluids has been described by Yuguchi et al. (2015, 2019). Myrmekites formed at temperature conditions below 500 °C based on ternary feldspar thermometry (Yuguchi et al.,

115 2011B). Petrography shows that plagioclase alteration does not occur at rims in contact
116 with K-feldspar, and the myrmekites were formed prior to the plagioclase alteration
117 (Yuguchi et al., 2019). Importantly, this study revealed a mass transfer that was higher than
118 that revealed by Yuguchi et al. (2015, 2019). Mass transfer through the myrmekitization
119 process, the chloritization process, and the plagioclase alteration process can provide
120 significant clues regarding the nature of the sequential and long-term variations in fluid
121 chemistry in granitic pluton across a wide temperature range during sub-solidus cooling.

122 This study constructed formation reactions for single myrmekite and composite
123 myrmekites based on a combination of petrography, mineral chemistry, image processing,
124 and singular value decomposition for the myrmekites in undeformed Toki granite in order
125 to decipher the following nature: (1) a quantitative estimate of mass transfer between the
126 reactant and product minerals, and the inflow and outflow of components with
127 consideration of the volume change due to micropore formation, (2) the factor controlling
128 the formation of micropores during myrmekitization, and (3) the sequential variations in the
129 hydrothermal fluid chemistry during sub-solidus conditions.
130

This is the peer-reviewed, final accepted version for American Mineralogist, published by the Mineralogical Society of America.
The published version is subject to change. Cite as Authors (Year) Title. American Mineralogist, in press.
DOI: https://doi.org/10.2138/am-2021-7956. http://www.minsocam.org/

THE TOKI GRANITE

The Toki granite in the Tono district of central Japan is one of the Late Cretaceous plutonic bodies of the Sanyo Belt in the Inner Zone (northern side of the Median Tectonic Line) of the Southwest Japan Arc (Fig. 1A; Ishihara, 2003; Ishihara and Chappell, 2007). This granitic pluton occurs as a stock of approximately 14 × 12 km^2 (Ishihara and Suzuki, 1969) that intrudes into the Jurassic sedimentary rocks of the Kamiaso unit in the Mino Terrane (Sano et al., 1992) and the Nohi Rhyolite (Sonehara and Harayama, 2007) (Fig. 1B); it is overlain unconformably by the Miocene Mizunami Group and the Mio-Pleistocene Tokai Group (Itoigawa, 1974, 1980; Todo Collaborative Research Group, 1999). The Toki granite is a zoned pluton consisting of three rock facies grading from muscovite–biotite granite (MBG) at the margin, through hornblende–biotite granite (HBG), to biotite granite (BG) in the interior (Fig. 1C; Yuguchi et al., 2010). Pegmatites and aplites occur as veins and dikes (Yuguchi et al., 2011B). The extent of myrmekite growth can be used as an indicator of the cooling process of the Toki granite (Yuguchi et al., 2011A, 2011B). The systematic variation in the development of the myrmekite indicates that the Toki granite cooled effectively from the roof and from the western margin during the deuteric stage (Yuguchi et al., 2011B).

This is the peer-reviewed, final accepted version for American Mineralogist, published by the Mineralogical Society of America.
The published version is subject to change. Cite as Authors (Year) Title. American Mineralogist, in press.
DOI: https://doi.org/10.2138/am-2021-7956. http://www.minsocam.org/

SAMPLING AND ANALYTICAL PROCEDURES

Twelve samples were collected from six boreholes in the Toki granite for this study (Fig. 1C). Sample Nos. 1–3 and 6 were collected from the MBG lithofacies, sample Nos. 7–9 and 12 were collected from HBG, and sample Nos. 4, 5, 10, and 11 were collected from BG.

This study presents petrography, mineral chemistry, image processing, and singular value decomposition results. The data used for petrography in this study were obtained from two-dimensional thin sections that were prepared carefully to prevent the detachment of minerals. Backscattered electron (BSE) images and elemental maps were generated using a JEOL IT100A scanning electron microscope (SEM) equipped with an energy-dispersive X-ray spectrometer at Yamagata University, operating at an acceleration voltage of 15 kV and a beam current of 1.0 nA. Mineral compositions were analyzed by using an electron microprobe analyzer (JEOL JXA-8900) with a wavelength-dispersive X-ray spectrometer (WDS) at Yamagata University. The analytical conditions required for the quantitative analysis were as follows: an acceleration voltage of 15 kV, beam current of 20 nA, beam diameter of 3 μm, and application of the ZAF data correction method (Kinouchi, 2001).

The area of the micropores and the product minerals in the myrmekite was determined through image processing analysis. The image analysis procedure using the image processing software Adobe Photoshop® is illustrated in Fig. S1. For example, sample MIU2-34 M11 had a myrmekite area of 19,970 μm^2, which included 18,228 μm^2 of albite-rich plagioclase in myrmekite (referred to as myrmekitic plagioclase), 1,189 μm^2 of

This is the peer-reviewed, final accepted version for American Mineralogist, published by the Mineralogical Society of America.
The published version is subject to change. Cite as Authors (Year) Title. American Mineralogist, in press.
DOI: https://doi.org/10.2138/am-2021-7956. http://www.minsocam.org/

171 vermicular quartz, 62 μm^2 of K-feldspar in myrmekite (myrmekitic K-feldspar), and 491
172 μm^2 of micropores (Fig. S1). In the BSE image, linear voids within myrmekite, which did
173 not penetrate from the myrmekite layer to neighbouring minerals, were identified as
174 micropores because the cross-sections of the tube-shaped micropores could be observed as
175 linear voids. On the other hand, long linear voids extending from the myrmekite layer to
176 neighbouring minerals were identified as microcracks and were eliminated from the area
177 counts of micropores.

178 We established the reaction equations based on the singular value decomposition (e.g.,
179 Fisher, 1989, 1993). The singular value decomposition technique is closely related to the
180 least square method. The least-square regression is an approach in regression analysis for
181 determining the solution of overdetermined equations, which enables the determination of
182 the precise mass balance relationships in multicomponent mineral assemblages based on
183 mineral analyses with possible analytical errors (Fisher, 1989). Cesare et al. (2002)
184 presented the singular value decomposition method for myrmekite formation. This singular
185 value decomposition method can also be used to analyse open-system reactions (Shigeno et
186 al., 2012). Yuguchi et al. (2015, 2019) applied the singular value decomposition method to
187 model the possible reaction relationships satisfying the volume relationship between
188 reactants and products during biotite chloritization and plagioclase alteration. Thus,
189 singular value decomposition can be applied to study the differences between the three
190 types of myrmekite formation satisfying the volume relationship between reactants and
191 products in an open system.
192

193 # PETROGRAPHY

194 ## Mineralogy of the samples

195 The mineral assemblage in the studied samples consists of quartz + plagioclase +
196 K-feldspar + biotite ± hornblende ± muscovite, with accessory minerals such as zircon,
197 apatite, ilmenite, magnetite, and secondary minerals such as chlorite, titanite, epidote,
198 allanite, sericite, and calcite. Quartz occurs as euhedral to anhedral crystals with 0.5–20
199 mm across, ranging from 24.0 to 40.3 vol% in each thin section. Plagioclase (19.7 to 35.6
200 vol%) occurs as subhedral to euhedral crystals, 1–20 mm across with normal zonation.
201 K-feldspar (27.2 to 44.4 vol%) occurs as subhedral crystals, 1–40 mm across with perthitic
202 texture. Biotite is variably altered and is partially or wholly replaced by chlorite. The modes
203 of biotite and hornblende in each thin section range from 0.5 to 5.2 vol% and from 0.1 to
204 0.6 vol%, respectively. Muscovite occurs as fine grain 0.1–1.0 mm across with a mode
205 below 0.5 vol%.
206
207 ## Three types of myrmekites: Morphology and mineral chemistry
208 The following three types of myrmekites occur within the Toki granite.
209 **Type A.** Type A myrmekite is defined as a single-layer myrmekite that developed
210 between magmatic plagioclase and K-feldspar (Figs. 2A and S2A−D). This type occurs the
211 most frequently among the three types. Vermicular quartz occurs as bead-like and rod-like
212 shapes less than 8 μm in width, which are elongated perpendicular to the boundary between
213 myrmekite and K-feldspar (Fig. 2A). The elemental composition of myrmekitic plagioclase
214 ranges from Ab_{86} to Ab_{97}, with a constant orthoclase component of $Or_{1\text{-}2}$ (Fig. 2B). Figure

This is the peer-reviewed, final accepted version for American Mineralogist, published by the Mineralogical Society of America.
The published version is subject to change. Cite as Authors (Year) Title. American Mineralogist, in press.
DOI: https://doi.org/10.2138/am-2021-7956. http://www.minsocam.org/

215 2C shows the BSE images with the scanning lines and compositional profiles along them.
216 The line profile across Type A myrmekite from magmatic plagioclase to magmatic
217 K-feldspar demonstrates the compositional variation from Ab_{86} at the plagioclase rim in
218 contact with myrmekite, through Ab_{86-97} for the myrmekitic plagioclase, to Or_{98} for the
219 K-feldspar rim (Fig. 2C).
220
221 **Type B.** Type B myrmekite is defined as composite layers of the myrmekite layer and
222 an Ab-rich layer (Figs. 3A, 3B and S2E). The Ab-rich layer does not contain vermicular
223 quartz. Type B myrmekite consists of two layers developed between magmatic plagioclase
224 and K-feldspar, that is, it can be subdivided into the following two sub-types: a myrmekite
225 layer in contact with magmatic K-feldspar (Fig. 3A-1 and B-1) and a myrmekite layer at the
226 side of magmatic plagioclase (Fig. 3A-2 and B-2). The chemical composition of
227 myrmekitic plagioclase in Type B ranges from Ab_{80} to $Ab_{89,}$ and it is below Or_1 (Fig. 3C).
228 Vermicular quartz occurs as bead-like and rod-like shapes less than 8 μm in width, and
229 these are elongated perpendicular to the boundary between myrmekite and K-feldspar (Fig.
230 3A). The Ab-rich layer of Type B has a chemical composition ranging from Ab_{89} to Ab_{98},
231 with constant orthoclase components below Or_1 (Fig. 3D). The line profile of Type B
232 myrmekite shows compositional variations from Ab_{83-84} at the rim of magmatic plagioclase,
233 Ab_{94-99} in the Ab-rich layer, Ab_{82-89} in the myrmekitic plagioclase, and Or_{95} at the rim of
234 magmatic K-feldspar (Fig. 3D).
235
236 **Type C.** Type C myrmekite consists of three layers, which are developed from the

This is the peer-reviewed, final accepted version for American Mineralogist, published by the Mineralogical Society of America.
The published version is subject to change. Cite as Authors (Year) Title. American Mineralogist, in press.
DOI: https://doi.org/10.2138/am-2021-7956. http://www.minsocam.org/

plagioclase side myrmekite layer (PML), through the Ab-rich layer, to the K-feldspar side myrmekite layer (KML) (Figs. 4A, 4B and S2F). Type C is only observed in sample DH13-8 M10. Vermicular quartz occurs with bead-like and rod-like shapes less than 10 μm in width at the PML and 5 μm in width at the KML, both of which are elongated perpendicular to the layer boundary (Fig. 4A). Although the growth length of vermicular quartz is longer in the PML than that in the KML, the frequency of the vermicular quartz is lower in the PML. In the PML, the myrmekitic plagioclase composition ranges from Ab_{85} to Ab_{92}, with a constant value of the orthoclase component below Or_2 (Fig. 4C). The KML has myrmekitic plagioclase with an albite component of $Ab_{83–88}$ and an orthoclase component below Or_1 (Fig. 4C). The chemical composition of the Ab-rich layer in Type C ranges from Ab_{93} to Ab_{95}, with an orthoclase component below Or_1 (Fig. 4C). The line profile of Type C myrmekite shows the compositional variation of Ab_{83-85} at the rim of the magmatic plagioclase, Ab_{87-92} in the myrmekitic plagioclase in the PML, Ab_{94-95} in the Ab-rich layer, Ab_{83-86} in the myrmekitic plagioclase in the KML, and Or_{93-96} at the rim of magmatic K-feldspar (Fig. 4D).

Ab-rich rim

The Ab-rich rim is defined as a single-layer plagioclase with no vermicular quartz that has developed between magmatic plagioclase and K-feldspar (Fig. S3). Figure S3 shows the BSE images with the scanning lines and compositional profiles along them. The line profile across the Ab-rich rim from magmatic plagioclase to magmatic K-feldspar demonstrates the compositional variation from Ab_{75-80} at the plagioclase rim in contact with

This is the peer-reviewed, final accepted version for American Mineralogist, published by the Mineralogical Society of America.
The published version is subject to change. Cite as Authors (Year) Title. American Mineralogist, in press.
DOI: https://doi.org/10.2138/am-2021-7956. http://www.minsocam.org/

the Ab-rich rim, through Ab_{93-99} for the Ab-rich rim, to Or_{98} for the K-feldspar rim (Fig. S3).

Micropores

In the three types of myrmekites, both myrmekitic plagioclase and vermicular quartz include micropores that have angular and rounded shapes less than 3 μm in size along their major axis (Fig. 5). The myrmekitic plagioclase contains more micropores than the vermicular quartz (Figs. 5 and 6). A large area of micropores occurs in the myrmekitic plagioclase in contact with the vermicular quartz (Fig. 5). The Ab-rich layers in Type B and C (Fig. 5B-2 and C-2) and the Ab-rich rim (Fig. S3) have few or no micropores. In Type B and C, the difference in micropore frequency between the myrmekite layer and the neighbouring Ab-rich layer indicates that the production of micropores could not be attributed to the detachment of feldspar during the preparation of the thin section.

K-feldspar occurrence in myrmekite and the Ab-rich rim

This study has newly found K-feldspar in Type A–C myrmekites, and it occurs both within the vermicular quartz (Fig. 6A and B) and between vermicular quartz and myrmekitic plagioclase (Fig. 6C). Myrmekites with or without K-feldspar are observed with equal frequency in the samples of the Toki granite. The K-feldspar grains within the vermicular quartz are less than 3 μm in width, and these are elongated parallel to the elongation direction of the vermicular quartz (Fig. 6A and B). The K-feldspar grains within the vermicular quartz are accompanied by no micropores at a higher frequency (Fig. 6A)

This is the peer-reviewed, final accepted version for American Mineralogist, published by the Mineralogical Society of America.
The published version is subject to change. Cite as Authors (Year) Title. American Mineralogist, in press.
DOI: https://doi.org/10.2138/am-2021-7956. http://www.minsocam.org/

and micropores at a lower frequency (Fig. 6B). Although its paucity of K-feldspar prevented an accurate quantitative analysis with an electron microprobe, the elemental maps showing the elemental Si, Al, Na, and K concentrations indicated that the composition of K-feldspar in the vermicular quartz does not differ from the composition of magmatic K-feldspar (Fig. 6A-2, B-2, and C-2). The K-feldspar in the myrmekitic plagioclase shows bead-like and amoeba-like shapes with irregular boundaries (Fig. 6C). The K-feldspar does not include micropores. The chemical composition of K-feldspar in the myrmekitic plagioclase has $Or_{95}Ab_5$, which is consistent with that of magmatic K-feldspar (DH13-8 M10 B2 and A2 of Table 1). The Ab-rich rim (layer) also includes K-feldspar grains, which are less than 3 μm in width (Fig. S3). Figure 3 shows that K-feldspar grains are observed in the Ab-rich rim in contact with magmatic plagioclase. The K-feldspar grains are accompanied by no micropores.

This is the peer-reviewed, final accepted version for American Mineralogist, published by the Mineralogical Society of America.
The published version is subject to change. Cite as Authors (Year) Title. American Mineralogist, in press.
DOI: https://doi.org/10.2138/am-2021-7956. http://www.minsocam.org/

294 # DISCUSSION

295 ## Micropores and K-feldspar in relation to myrmekite formation

296 The volume of micropores in Type A myrmekite was estimated from their area by
297 simply assuming the area–volume equivalence, which was determined through the image
298 processing analysis. Figure 7 shows the relationship between the micropore area and the
299 vermicular quartz area (A), and that between the micropore area and the myrmekitic
300 plagioclase (B), which exhibit high correlations (A: R^2 = 0.8352 and B: R^2 = 0.8642).
301 Therefore, the genesis of micropores is apparently related to the formation of myrmekites.
302 In particular, the Ab-rich layer has few or no micropores, thus indicating that the formation
303 of micropores is related to the formation of vermicular quartz.

304 The volume fractions of micropores in the myrmekite areas of Type A–C were also
305 determined by image processing analysis. The volume decrease between the reactant and
306 product minerals was defined as the volume fraction of the micropores in the myrmekite
307 area. The image analyses revealed a volume decrease from the reactant minerals to the
308 products as follows: 2.52% in Type A (MIU2-34 M13); 2.45% for the myrmekite layer and
309 0.00% for the Ab-rich layer in Type B (DH13-15 M11); and 1.29% for the PML, 0.04% for
310 the Ab-rich layer, and 4.68% for the KML in Type C (DH13-8 M10: Table 2).

311 Petrography results show that (1) K-feldspar is included within the core parts of
312 vermicular quartz (Fig. 6A and B), and (2) K-feldspar occurs in contact with vermicular
313 quartz (Fig. 6C). These occurrences of K-feldspar indicate that the formation of K-feldspar
314 is related to that of vermicular quartz. That is, the K-feldspar originated from myrmekite
315 formation, and it is referred to as “myrmekitic K-feldspar” hereafter.

This is the peer-reviewed, final accepted version for American Mineralogist, published by the Mineralogical Society of America.
The published version is subject to change. Cite as Authors (Year) Title. American Mineralogist, in press.
DOI: https://doi.org/10.2138/am-2021-7956. http://www.minsocam.org/

316

317 **Reactions leading to Type A–C myrmekites**

318 The formation of Type A–C myrmekites can be described by reaction equations that
319 represent the quantitative mass transfer between the reactant and product minerals, and the
320 inflow and outflow of components. The reaction equations were constructed for (1) sample
321 MIU2-34 M13 in the formation of Type A myrmekite, (2) sample DH13-15 M11 of Type B
322 myrmekite, and (3) sample DH13-8 M10 of Type C myrmekite.

323

324 **Type A myrmekite.** In the formation reaction of sample MIU2-34 M13 (Fig. 2), the
325 reactants include magmatic plagioclase and K-feldspar (analysis No. MIU2-34 M13 A1 and
326 A20 in Table 1) and the products include myrmekitic plagioclase (No. A15), vermicular
327 quartz (the ideal SiO_2 was assumed), and myrmekitic K-feldspar (the composition of
328 magmatic K-feldspar of No. A20 was used because of the similarity in the elemental map of
329 Fig. 6A). First, we considered the following reaction in a closed system:

$$a\,[Pl] + b\,[Kfs] = c\,[MP] + d\,[VQ] + e\,[MKfs]$$

330 where [Pl], [Kfs], [MP], [VQ], and [MKfs] denote the magmatic plagioclase, magmatic
331 K-feldspar, myrmekitic plagioclase, vermicular quartz, and myrmekitic K-feldspar,
332 respectively. To determine the stoichiometric coefficients a, b, c, d, and e in a closed system,
333 the conservations of all closure components (SiO_2, Al_2O_3, CaO, Na_2O, and K_2O) were
334 imposed as follows:

335 $2.88\,a + 3.00\,b = 2.91\,c + 1.00\,d + 3.00\,e$ (Closure of Si_2O)

336 $1.12\,a + 0.98\,b = 1.09\,c + 0.98\,e$ (Closure of Al_2O_3)

This is the peer-reviewed, final accepted version for American Mineralogist, published by the Mineralogical Society of America.
The published version is subject to change. Cite as Authors (Year) Title. American Mineralogist, in press.
DOI: https://doi.org/10.2138/am-2021-7956. http://www.minsocam.org/

337 $0.12\,a = 0.09\,c$ (Closure of CaO)

338 $0.85\,a + 0.03\,b = 0.90\,c + 0.03\,e$ (Closure of Na_2O)

339 $0.02\,a + 1.00\,b = 0.01\,c + 1.00\,e$ (Closure of K_2O)

340 There was no solution (stoichiometric coefficients) that satisfied the above five equations,
341 which indicates that myrmekite formation did not occur in the closed system.

342 Second, we considered the following reaction in an open system:

$$a\,[Pl] + b\,[Kfs] + X = c\,[MP] + d\,[VQ] + e\,[MKfs] + Y$$

343 where X and Y denote the inflow and outflow of chemical components through the
344 hydrothermal fluid. Ashworth (1972) described that the myrmekite developed by calcium,
345 sodium, and potassium exchange, and that both silicon and aluminium remained constant in
346 the system. The conservation of silicon and aluminium was also employed by Menegon et
347 al. (2006) and Abart et al. (2014). Therefore, we employed the conservation of SiO_2 and
348 Al_2O_3 to determine the absolute values of *a*, *b*, *c* (normalized to unity: *c* = 1), *d*, and *e* in the
349 reaction equation for Type A. As an additional condition, the volume ratios of the product
350 minerals in the myrmekite were used as candidates. The molar volumes of the reactant and
351 product minerals were derived from their chemical compositions (Table 1). The volume
352 fractions of the product minerals were expressed as ratios, such as myrmekitic
353 plagioclase:vermicular quartz:myrmekitic K-feldspar = 1:0.065:0.003 (Table 2).
354 Stoichiometric coefficients of open components were calculated based on the values of *a*, *b*,
355 *c*, *d*, and *e*, and the following reaction was obtained:

356 0.318 [Pl] + 0.751 [Kfs] + 0.607 Na^+ + 0.052 Ca^{2+} → 1 [MP] + 0.252 [VQ] + 0.003
357 [MKfs] + 0.745 K^+…reaction (A1)

This is the peer-reviewed, final accepted version for American Mineralogist, published by the Mineralogical Society of America.
The published version is subject to change. Cite as Authors (Year) Title. American Mineralogist, in press.
DOI: https://doi.org/10.2138/am-2021-7956. http://www.minsocam.org/

Reaction (A1) demonstrates the myrmekite formed by consumption of two feldspars with inflows of Na^+ and Ca^{2+} associated with the removal of K^+ through an intergranular medium. Reaction (A1) is also characterized by a volume decrease of approximately 5.60% from reactants to products based on the molar volumes and stoichiometric coefficients of the reactant and product. Such a volume decrease (5.60%) is not consistent with the volume decrease (2.52%) based on the image analysis of micropores from the reactants to the products in Type A. That is, reaction (A1) could not explain the myrmekite petrography.

Third, we did not specify the conservation of closure components, and therefore, singular value decomposition was employed to determine the reaction equations in an open system. In the singular value decomposition method, the reaction that satisfied both the volume relationship between the reactants and products (volume decrease of 2.52% in Type A) and the volume ratios of the product minerals (vermicular quartz:myrmekitic K-feldspar = 1:0.065:0.003) was derived (Table 2). The singular value decomposition method was used to determine the stoichiometric coefficients *a*, *b*, *c*, *d*, and *e* and those of the open components involved in X and Y. The matrices for singular value decomposition consisted of combinations of the volume relationship between the reactants and products, and the volume ratios of the product minerals (Table S1). The free software program Scilab (Scilab Enterprises S.A.S) was employed to perform the singular value decomposition. Silicon species occur in the form of H_4SiO_4 in the reaction equation. The singular value decomposition yielded the following reaction:

$$0.595\ [Pl] + 0.227\ [Kfs] + 0.047\ H_4SiO_4 + 0.181\ Na^+ + 0.207\ H^+ \rightarrow 0.771\ [MP] + 0.194\ [VQ] + 0.002\ [MKfs] + 0.047\ Al^{3+} + 0.002\ Ca^{2+} + 0.229\ K^+ + 0.198\ H_2O \ldots \text{reaction (A2)}$$

This is the peer-reviewed, final accepted version for American Mineralogist, published by the Mineralogical Society of America.
The published version is subject to change. Cite as Authors (Year) Title. American Mineralogist, in press.
DOI: https://doi.org/10.2138/am-2021-7956. http://www.minsocam.org/

380

381 **Type B myrmekite**

382 In Type B myrmekite (Fig. 3), the reactants are magmatic plagioclase and K-feldspar
383 (analysis No. DH13-15 A24 and A1 in Table 1), and the products are myrmekitic
384 plagioclase (No. A10), vermicular quartz (the ideal SiO_2 was assumed) in the myrmekite
385 layer, and the Ab-rich layer (No. A16). The following volume decreases from the reactants
386 to the products were imposed in the matrices of the singular value decomposition: 2.45% at
387 the myrmekite layer and 0.00% (volume constant) in the Ab-rich layer in Type B (Table 2).
388 The volume fractions of the layers were expressed as ratios, such as the myrmekite
389 layer:Ab-rich layer = 1:2.414, and the ratio of the product minerals was expressed as
390 myrmekitic plagioclase:vermicular quartz:Ab-rich layer = 0.916:0.084:2.414 (Table 2). We
391 considered the following reaction in an open system:

$$a\,[Pl] + b\,[Kfs] + X = c\,[MP] + d\,[VQ] + e\,[Ab] + Y\ (Ab{:}\ Ab-rich\ layer)$$

392 The singular value decomposition yielded the following reaction:

393 0.695 [Pl] + 0.201 [Kfs] + 0.086 H_4SiO_4 + 0.261 Na^+ + 0.182 H^+ → 0.243 [MP] + 0.086
394 [VQ] + 0.641 [Ab] + 0.055 Al^{3+} + 0.045 Ca^{2+} + 0.198 K^+ + 0.262 H_2O…reaction (B)

395

396 **Type C myrmekite**

397 In Type C myrmekite (Fig. 4), the reactants are plagioclase (analysis No. DH13-8 A23
398 in Table 1) and K-feldspar (No. A2). The products are myrmekitic plagioclase (PML-MP:
399 No. A15), vermicular quartz (PML-VQ: the ideal SiO_2 was assumed), and myrmekitic
400 K-feldspar (PML-MKfs: No. B2) in the PML, as well as the Ab-rich layer (Ab: No. A11),

This is the peer-reviewed, final accepted version for American Mineralogist, published by the Mineralogical Society of America.
The published version is subject to change. Cite as Authors (Year) Title. American Mineralogist, in press.
DOI: https://doi.org/10.2138/am-2021-7956. http://www.minsocam.org/

myrmekitic plagioclase (KML-MP: No. A8), and vermicular quartz (KML-VQ: the ideal SiO_2 was assumed) in the KML. The following volume decreases from the reactants to the products were imposed in the matrices of the singular value decomposition method: 1.29% at the PML, 0.04% in the Ab-rich layer, and 4.68% in the KML in Type C (Table 2). The volume fractions of the layers were expressed as ratios, such as the KML:Ab-rich layer:PML = 1:0.681:3.688, and the ratio of the products was expressed as KML-MP:KML-VQ:Ab:KML-MP:KML-VQ:KML-Kfs = 0.898:0.102:0.651:3.388:0.236:0.064 (Table 2). We considered the following reaction in an open system:

$$a\,[Pl] + b\,[Kfs] + X = c\,[KML-MP] + d\,[KML-VQ] + e\,[Ab] + f\,[PML-MP] + g\,[PML-VQ] + h\,[PML-Mkfs] + Y$$

The singular value decomposition yielded the following reaction:

$$0.972\ [Pl] + 0.145\ [Kfs] + 0.071\ H_4SiO_4 + 0.086\ Na^+ + 0.466\ H^+ \rightarrow 0.187\ [KML\text{-}MP] + 0.082\ [KML\text{-}VQ] + 0.135\ [Ab] + 0.704\ [PML\text{-}MP] + 0.190\ [PML\text{-}VQ] + 0.012\ [PML\text{-}MKfs] + 0.116\ Al^{3+} + 0.041\ Ca^{2+} + 0.135\ K^+ + 0.384\ H_2O \ldots \text{reaction (C)}$$

Mass transfer between reactants and hydrothermal fluid during myrmekitization

The reactions (A2), (B), and (C) are commonly characterized by the production of myrmekite through the consumption of plagioclase and K-feldspar with an inflow of H_4SiO_4, Na^+, and H^+ from the hydrothermal fluid, accompanied by an outflow of Al^{3+}, Ca^{2+}, and K^+ into the fluid. This represents an essential mass transfer for myrmekite formation. Hydrogen ions can be observed as a reactant (left-hand side) in reactions (A2), (B), and (C).

This is the peer-reviewed, final accepted version for American Mineralogist, published by the Mineralogical Society of America.
The published version is subject to change. Cite as Authors (Year) Title. American Mineralogist, in press.
DOI: https://doi.org/10.2138/am-2021-7956. http://www.minsocam.org/

Therefore, there is a gradual decrease in the H^+ concentration of the hydrothermal fluid as the myrmekite growth proceeds, thus producing a gradual increase in pH in the hydrothermal fluid. A hydrothermal fluid with a high pH enhances the decomposition of feldspar (Yasuhara et al., 2012). The reaction extent was constrained by the inflow of H_4SiO_4 or Na^+ in the fluids. That is, a reduction in the H_4SiO_4 or Na^+ supply will cause the termination of the myrmekitization reaction. The differences among reactions (A2), (B), and (C) demonstrate the predominant factors leading to the difference in the formation of Types A, B, and C; (1) sums of reactant amounts (volume) increase from Type A through Type B to Type C; and (2) the ratio of plagioclase in reactants increases from Type A through Type B to Type C. The volumes of the reactant feldspars of the composite myrmekite are larger than those of single myrmekite (reactions (A2), (B), and (C)). If the stoichiometric coefficients of myrmekitic plagioclase in Types A, B, and C (KML-MP) are normalized to 1, those of reactant feldspars are 1.066 (0.772 for plagioclase and 0.294 for K-feldspar) in Type A, 3.687 (2.860 of plagioclase and 0.827 of K-feldspar) in Type B, and 5.973 (5.198 of plagioclase and 0.775 of K-feldspar) in Type C. The volumes of reactant feldspars are 84.4 cm^3, 91.7 cm^3, and 113.4 cm^3 in Types A, B and C, respectively, which were calculated by using the stoichiometric coefficients of reactants (reactions (A2), (B), and (C)) and their molar volumes (Table 1). The ratio of plagioclase consumption to K-feldspar consumption increases from Type A through Type B to Type C as follows: Pl:Kfs = 2.4:1 in Type A, Pl:Kfs = 3.2:1 in Type B, and Pl:Kfs = 6.2:1 in Type C. The composite myrmekite requires larger amounts of plagioclase consumption relative to K-feldspar consumption than the single myrmekite. In summary, the progression of the

445 reaction resulted in high pH conditions in the hydrothermal fluid and thus the
446 decomposition of feldspars, which leads to the promotion of composite myrmekite. In
447 particular, the consumption of a large amount of plagioclase contributes to the formation of
448 composite myrmekite.
449
450 **Formation factors for micropores during myrmekitization**
451 To clarify the formation factors of micropores during myrmekitization, we derived the
452 reactions of Type A–C based on the assumption of a constant volume between reactants and
453 products (i.e., no production of micropores) with the volume ratios of the product minerals
454 (Table S2), for comparison to the reactions considering micropores (reactions (A2), (B),
455 and (C)). The differences in the reactions of Type A–C between the production of
456 micropores and the non-production of micropores are characterized by the following
457 features: (1) inflow amounts of H_4SiO_4 and Na^+ in the former reactions (reactions (A2), (B),
458 and (C)) are smaller than those in the latter reactions (Table S2), (2) the outflow amounts of
459 Al^{3+} and Ca^{2+} in the former reactions are larger than those in the latter reactions, and (3)
460 inflow amounts of H^+ in the former reactions are larger than those in the latter reactions.
461 The features (1) and (2) are consistent with the interpretations of Putnis (2015) on
462 micropore formation associated with plagioclase albitization. Putnis (2015) proposed that
463 some silica in the hydrothermal fluid must not participate in the reaction, and both calcium
464 and aluminium are released into the fluid to account for the micropores in plagioclase
465 albitization because the reactant plagioclase has the same molar volume as albite. However,
466 the features (1) and (2) cannot explain the observations in which high-frequency

467 micropores occur in the myrmekite layer but few micropores occur in the Ab-rich rim
468 (layer). Thus, not only features (1) and (2) but also feature (3) are significant factors for the
469 production of the micropores during the formation processes of myrmekite.

470 We constructed the reaction equation of the Ab-rich rim based on the assumption of a
471 slight volume decrease of 0.003% from reactants to products with the volume ratios of the
472 product minerals (Table S3). The reactions of the Ab-rich rim and Type A myrmekite
473 (reaction (A2)) can lead to the differences found for the formation factors between the
474 occurrence and non-occurrence of micropores. In the reaction equations, the hydrogen ions
475 are observed as a reactant (left-hand side). The inflow amount of H^+ in Type A (0.207 in
476 terms of the stoichiometric coefficient) is higher than that in the Ab-rich rim (0.059). Such
477 an observation in the reaction equations is consistent with feature (3). Therefore, the
478 formation of micropores is accompanied by a larger inflow of H^+, i.e., lower pH conditions
479 in the hydrothermal fluid were required. In summary, smaller inflows of H_4SiO_4 and Na^+
480 from the hydrothermal fluid with lower pH conditions yielded micropore production during
481 myrmekitization, and this is accompanied by larger outflows of Al^{3+} and Ca^{2+}. Meanwhile,
482 larger inflows of H_4SiO_4 and Na^+ from the hydrothermal fluid with higher pH conditions
483 yielded the formation of an Ab-rich rim (layer) without micropores, and this is
484 accompanied by smaller outflows of Al^{3+} and Ca^{2+}. Such interpretations are consistent with
485 the finding that the necessary condition for formation of the composite myrmekite is the
486 high pH conditions of hydrothermal fluid because the composite myrmekite includes the
487 Ab-rich layer. Conversely, the presence or absence of micropores can be used as a
488 significant indicator for evaluations of the pH conditions in the hydrothermal fluid.

This is the peer-reviewed, final accepted version for American Mineralogist, published by the Mineralogical Society of America.
The published version is subject to change. Cite as Authors (Year) Title. American Mineralogist, in press.
DOI: https://doi.org/10.2138/am-2021-7956. http://www.minsocam.org/

489

490 **Sequential variations in the hydrothermal fluid chemistry during sub-solidus**
491 **conditions**

492 The production of myrmekite is characterized by the consumption of plagioclase and
493 K-feldspar with an inflow of H_4SiO_4, Na^+, and H^+ from the hydrothermal fluid, and this
494 accompanied by an outflow of Al^{3+}, Ca^{2+}, and K^+ into the fluid (Fig. 8). Mass transfers with
495 myrmekitization occur at higher temperature conditions than those for biotite chloritization
496 and plagioclase alteration (Yuguchi et al., 2011B, 2015, 2019). The characteristics of mass
497 transfer during biotite chloritization and plagioclase alteration were described in Yuguchi et
498 al. (2015, 2019), respectively. Figure 8 schematically shows the mass transfer of chemical
499 components through hydrothermal fluids during myrmekitization, biotite chloritization, and
500 plagioclase alteration, and the data demonstrate the sequential variations in the
501 hydrothermal fluid chemistry during sub-solidus conditions. The concentrations of H_4SiO_4,
502 Na^+, and H^+ in the fluid decreased gradually, while those of Al^{3+}, Ca^{2+}, and K^+ increased
503 gradually as myrmekitization proceeds. The inflow of Al^{3+}, Fe^{2+}, Mn^{2+}, and Ca^{2+} was
504 required in biotite chloritization (Yuguchi et al., 2015), and the inflow of H_4SiO_4 (Si^{4+}), K^+,
505 Al^{3+}, Fe^{2+}, Mn^{2+}, and Mg^{2+} was required in plagioclase alteration (Yuguchi et al., 2019).
506 The outflow components with myrmekitization may be used in biotite chloritization and
507 plagioclase alteration. The biotite chloritization and plagioclase alteration yielded the
508 following variations in fluid chemistry: a gradual decrease in Al^{3+}, Fe^{2+}, Mn^{2+}, and Mg^{2+}
509 and a gradual increase in Ca^{2+}, K^+, H^+, and F^- (Yuguchi et al., 2015, 2019). In summary, the
510 sequential variations in the chemical characteristics of the hydrothermal fluid of the Toki

granite were characterized by the gradual decrease in H_4SiO_4 (Si^{4+}), Fe^{2+}, Mn^{2+}, Mg^{2+}, and Na^+ and the gradual increase in Ca^{2+}, K^+, H^+, and F^-.

IMPLICATION

The methodology and interpretations in this study provide new insights into the mechanism of myrmekite formation in a granitic system. This study employed an approach that combined petrography, mineral chemistry, image processing, and the singular value decomposition method of the myrmekites in undeformed Toki granite, and the results led to an increased understanding of (1) a quantitative estimate of mass transfer between the reactant and product minerals, and the inflow and outflow of components with consideration of the volume change due to micropore formation, (2) the factor controlling the formation of micropores during myrmekitization, and (3) the sequential variations in the hydrothermal fluid chemistry during sub-solidus conditions. The petrography revealed the presence of micropores in the myrmekites, and this study clarified that the genesis of micropores is related to the formation of myrmekites, which was accomplished by employing an image processing methodology to evaluate the areas of micropores, vermicular quartz, and myrmekitic plagioclase. In the undeformed granite, the image processing analysis provided an accurate estimate of the volume fractions of micropores in the myrmekite area, that is, the volume decrease in the reaction. On the basis of the obtained volume relation, singular value decomposition was used to determine the myrmekite reactions from the reactants to the products, which can serve as an effective technique to reveal the mass transfer in the reaction of myrmekite formation with a volume change. Our results demonstrate that the recognition of micropores is important for the precise evaluation of mass transfer during myrmekitization. The micropores act as a migration pathway for hydrothermal fluid and thus enhance the mass transfer within a

granitic body starting with the myrmekite formation and continuing through the present day and into the future. Characterization of micropores within granitic rock can also contribute to safety evaluations for the geological disposal of nuclear waste and the geological storage of oil and natural gas.

ACKNOWLEDGEMENTS

Constructive reviews by two anonymous reviewers and Dr. T. Mueller (associated editor) were very helpful during revisions of the manuscript. This work was financially supported by the JSPS (Japan Society for the Promotion of Science) KAKENHI for Young Scientists program [grant number 16H06138] and by a grant from the Ministry of Economy, Trade and Industry (METI) to TY. We would also like to thank Editage (www.editage.jp) for English language editing.

548 **REFERENCES CITED**

549 Abart, R., Heuser, D., Habler, G. (2014) Mechanisms of myrmekite formation: case study
550 from the Weinsberg granite, Modanubian zone, Upper Austria. Contributions to
551 Mineralogy and Petrology, 168, 1074.

552 Ashworth J.R. (1972) Myrmekite of exsolution and replacement origins. Geological
553 Magazine, 109, 45–62.

554 Becke, F. (1908) Über Myrmekit. Mineralogische und Petrographische Mitteilungen, 27,
555 377–390.

556 Cesare, B., Marchesi, C., Connolly, J.A.D. (2002) Growth of myrmekite coronas by contact
557 metamorphism of granitic mylonites in the aureole of Cima di Vila, Eastern Alps, Italy.
558 Journal of Metamorphic Geology, 20, 203–213.

559 Cisneros-Lazaro, D., Miller, J.A., Baumgartner, L. (2019) Role of myrmekite and
560 associated deformation fabrics in controlling development of granitic mylonites in the
561 Pofadder Shear Zone of southern Namibia. Contributions to Mineralogy and Petrology,
562 174, 1–22.

563 Drescher-Kaden, F.K. (1948) Die Feldspat-Quarz-Reaktionsgefüge der Granite und Gneise
564 und ihre genetische Bedeutung. Springer-Verlag, Berlin, 259 pp.

565 Fisher, G.W. (1978) Rate laws in metamorphism. Geochimica et Cosmochimica Acta, 42,
566 1035–1050.

567 Fisher, G.W. (1989) Matrix analysis of metamorphic mineral assemblages and reactions.
568 Contributions to Mineralogy and Petrology, l02, 69–77.

569 Fisher, G.W. (1993) An improved method for algebraic analysis of metamorphic mineral

570 assemblages. American Mineralogist, 78, 1257–1261.
571 Gresens, R.L. (1967) Composition-volume relationships of metasomatism. Chemical
572 Geology, 2, 47–65.
573 Hövelmann, J., Putnis, A., Geisler, T., Schmidt, B.C., Golla-Schimdler, U. (2010) The
574 replacement of plagioclase feldspar by albite: observations form hydrothermal
575 experiments. Contributions to Mineralogy and Petrology, 159, 43–59.
576 Ishihara, S. (2003) Chemical contrast of the Late Cretaceous granitoids of the Sanyo and
577 Ryoke Belts, Southwest Japan: Okayama-Kagawa Transect. Bulletin of the Geological
578 Survey of Japan, 54, 95–116.
579 Ishihara, S., Suzuki, Y. (1969) Basement granites of the Toki uranium deposits in Tono
580 region. Reports Geological Survey of Japan, 232, 113–127.
581 Ishihara, S., Chappell, B. (2007) Chemical compositions of the late Cretaceous Ryoke
582 granitoids of the Chubu District, central Japan – Revisited. Bulletin of the Geological
583 Survey of Japan, 58, 323–350.
584 Itoigawa, J. (1974) Geology of the Mizunami district, central Japan. Bulletin Mizunami
585 Fossil Museum, 1, 9–42 (in Japanese).
586 Itoigawa, J. (1980) Geology of the Mizunami district, central Japan. Monograph of the
587 Mizunami Fossil Museum, 1, 1–50 (in Japanese).
588 Japan Nuclear Cycle Development Institute (2002) Master Plan of the Mizunami
589 Underground Research Laboratory Project. JNC Technical Report. JNC TN7410
590 2003-001, Tono Geoscience Center.
591 Joanny, V., Van Roermund, H.L.M., Lardeaux, J.M. (1991) The clinopyroxene/plagioclase

592 symplectite in retrograde eclogites: a potential geothermobarometer. Geologische
593 Rundschau 80, 303–320.
594 Kinouchi, S., (2001) Electron Probe Microanalyzer, Gijutsu-shoin, Tokyo, pp.346.
595 Menegon, L., Pennacchioni, G., Stunitz, H. (2006) Nucleation and growth of myrmekite
596 during ductile shear deformation in metagranites. Journal of Metamorphic Geology, 24,
597 553–568.
598 Phillips, E.R. (1974) Myrmekite-one hundred years later. Lithos, 7, 181–194.
599 Putnis, A. (2015) Transient porosity resulting from fluid-mineral interaction and its
600 consequences. Reviews in Mineralogy and Geochemistry, 80, 1–23.
601 Sano, H., Yamagata, T., Horibo, K. (1992) Tectonostratigraphy of Mino terrane: Jurassic
602 accretionary complex of southwest Japan. Palaeogeography, Palaeoclimatology,
603 Palaeoecology, 96, 41–57.
604 Schwanke, A. (1909) Die Beimischung von Ca in Kalifeldspatund die Myrmekitbildung.
605 Zentblatt für Mineralogie, 311–316.
606 Shelley, D. (1964) On myrmekite. American Mineralogist, 49, 41–52.
607 Shigeno, M., Mori, Y., Shimada, K., Nishiyama, T. (2012) Jadeites with metasomatic
608 zoning from the Nishisonogi metamorphic rocks, western Japan: fluid-tectonic block
609 interaction during exhumation. European Journal of Mineralogy, 24, 289–311.
610 Sonehara, T., Harayama, S. (2007) Petrology of the Nohi Rhyolite and its related
611 granitoids: a Late Cretaceous large silicic igneous field in central Japan. Journal of
612 Volcanology and Geothermal Research, 167, 57–80.
613 Spencer E. (1938) The potash-soda-feldspars. II. Some applications to petrogenesis.

614 Mineral. Magazine, 25, 87–118.
615 Todo Collaborative Research Group (1999) Fault bounded inland basin of multiple blocks:
616 An example from the sedimentary basin of the Tokai Group around Tajimi City in Gifu
617 Prefecture, central Japan. Earth Science (Chikyu Kagaku), 53, 291–306 (in Japanese
618 with English abstract).
619 Yasuhara, H., Hashimoto, K., Kinoshita, N. (2012) Evaluation of dissolution equation in
620 granite examined by flow-through dissolution experiment under temperature and pH
621 conditions controlled. Journal of the Mining and Materials Processing Institute of Japan,
622 128, 79–85.
623 Yuguchi, T., Nishiyama, T. (2007) Cooling process of a granitic body deduced from the
624 extents of exsolution and deuteric sub-solidus reactions: Case study of the Okueyama
625 granitic body, Kyushu, Japan. Lithos, 97, 395–421.
626 Yuguchi, T., Nishiyama, T. (2008) The mechanism of myrmekite formation deduced from
627 steady-diffusion modelling based on petrography: Case study of the Okueyama granitic
628 body, Kyushu, Japan. Lithos, 106, 237–260.
629 Yuguchi, T., Sasao, E., Ishibashi, M., Nishiyama, T. (2015) Hydrothermal chloritization
630 process from biotite in the Toki granite, Central Japan: Temporal variation of chemical
631 characteristics in hydrothermal fluid associated with the chloritization. American
632 Mineralogist, 100, 1134–1152.
633 Yuguchi, T., Shoubuzawa, K., Ogita, Y., Yagi, K., Ishibashi, M., Sasao, E., Nishiyama, T.
634 (2019) Role of micropores, mass transfer, and reaction rate in the hydrothermal
635 alteration process of plagioclase in a granitic pluton. American Mineralogist, 104,

536–556.

Yuguchi, T., Tsuruta, T., Nishiyama, T. (2010) Zoning of rock facies and chemical composition in the Toki granitic body, Central Japan. Japanese Magazine of Mineralogical and Petrological Sciences, 39, 50–70 (in Japanese with English abstract).

Yuguchi, T., Tsuruta, T., Nishiyama, T. (2011A) Three-dimensional cooling pattern of a granitic pluton I: The study of exsolution sub-solidus reactions in the Toki granite, Central Japan. Journal of Mineralogical and Petrological Sciences, 106, 61–78.

Yuguchi, T., Tsuruta, T., Nishiyama, T. (2011B) Three-dimensional cooling pattern of a granitic pluton II: The study of deuteric sub-solidus reactions in the Toki granite, Central Japan. Journal of Mineralogical and Petrological Sciences, 106, 130–141.

This is the peer-reviewed, final accepted version for American Mineralogist, published by the Mineralogical Society of America.
The published version is subject to change. Cite as Authors (Year) Title. American Mineralogist, in press.
DOI: https://doi.org/10.2138/am-2021-7956. http://www.minsocam.org/

FIGURE CAPTIONS

Figure 1. The Toki granitic pluton and Mizunami Underground Research Laboratory. (A) Map of southwest Japan showing the location of the Toki granite (Tono district; square symbol) in central Japan, together with the distribution of the San-in, Sanyo, and Ryoke Belts in the inner zone of southwest Japan, after Ishihara and Chappell (2007). (B) Geologic map of the Toki granite after Itoigawa (1980), the Mizunami Underground Research Laboratory, and the borehole sites. The topographic contours inside the Tono district are based on Geographical Survey Institute 1:25,000 topographic maps, titled "Mitake," "Takenami," "Toki," and "Mizunami." Borehole investigations of the Toki granite were performed by the Japan Atomic Energy Agency (Japan Nuclear Cycle Development Institute, 2002). (C) Rock facies cross-section of the Toki granite along the line from X to X' on the geologic map (Fig. 1B). MBG: muscovite–biotite granite, HBG: hornblende–biotite granite, and BG: biotite granite (Yuguchi et al., 2010). The lithofacies cross-sections also show the borehole locations (DH-6, 10, 11, 13, MIU2, and MIZ1) and sample locations (samples Nos. 1–12).

Figure 2. Type A (sample MIU2-34 M13). (A) Backscattered electron (BSE) image, (B) Or-Ab-An compositional plot of rims of magmatic plagioclase (Pl rim), myrmekitic plagioclase (Myr), and rims of magmatic K-feldspar (Kfs rim), and (C) compositional profiles along the scanning lines in the BSE image.

Figure 3. Type B (samples DH13-15 M11 and DH13-8 M05). (A) Backscattered electron

669 (BSE) image, (B) schematic figure, (C) Or-Ab-An compositional plot of rims of magmatic
670 plagioclase (Pl rim), myrmekitic plagioclase (Myr), Ab-rich layer, and rims of magmatic
671 K-feldspar (Kfs rim), and (D) compositional profiles along the scanning lines in the BSE
672 image (D: DH13-15 M11).
673
674 **Figure 4.** Type C (sample DH13-8 M10). (A) Backscattered electron (BSE) image, (B)
675 schematic figure, (C) Or-Ab-An compositional plot of rims of magmatic plagioclase (Pl
676 rim), myrmekitic plagioclase in the PML (PML-Myr), Ab-rich layer, myrmekitic
677 plagioclase in the KML (KML-Myr), and rims of magmatic K-feldspar (Kfs rim), and (D)
678 compositional profiles along the scanning lines in the BSE image.
679
680 **Figure 5.** Backscattered electron (BSE) images showing the distribution of micropores in
681 Type A–C myrmekites (A: sample MIU2-34 M13 of Type A; B: sample DH13-15 M11 of
682 Type B; and C: sample DH13-8 M10 of Type C).
683
684 **Figure 6.** Backscattered electron (BSE) images showing the myrmekitic K-feldspar of Type
685 A–C myrmekites with elemental maps showing the elemental Si, Al, Na, and K
686 concentrations (A: K-feldspar occurring in vermicular quartz with no micropores in sample
687 MIU2-34 M13; B: K-feldspar occurring in vermicular quartz with micropores in sample
688 DH6-28 M19; and C: K-feldspar occurring in myrmekitic plagioclase with no micropores
689 in sample DH13-8 M05).
690

691 **Figure 7.** (A) Dispersion diagram between the micropore area and the vermicular quartz
692 area, and (B) that between the micropore area and the myrmekitic plagioclase, which
693 produced good correlations (A: $R^2 = 0.84$ and B: $R^2 = 0.86$).
694
695 **Figure 8.** Schematic figure showing the mass transfer of chemical components through
696 hydrothermal fluids in myrmekitization, biotite chloritization, and plagioclase alteration
697 processes.
698
699 **Figure S1.** Image analysis revealing the area (μm^2) of the micropores, vermicular quartz,
700 myrmekitic plagioclase, and myrmekitic K-feldspar in the myrmekite, as determined by
701 image processing software using samples MIU2-34 M11 as examples. (A) The myrmekite
702 area was clipped from the backscattered electron BSE image using the image processing
703 software Photoshop®. (B to E) The areas of myrmekite, vermicular quartz, myrmekitic
704 K-feldspar, and micropores were extracted through binary image processing and counting
705 of the black pixels.
706
707 **Figure S2.** Polarization microphotographs of Type A myrmekite (A-C) and backscattered
708 electron (BSE) low-magnification images showing Type A (sample MIU2-34 M13: D), B
709 (DH13-15 M11: E), and C (DH13-8 M10: F).
710
711 **Figure S3.** Ab-rich rim (sample DH13-8 M6). BSE image and compositional profiles along
712 the scanning lines.

This is the peer-reviewed, final accepted version for American Mineralogist, published by the Mineralogical Society of America.
The published version is subject to change. Cite as Authors (Year) Title. American Mineralogist, in press.
DOI: https://doi.org/10.2138/am-2021-7956. http://www.minsocam.org/

Table 1 Representative compositions of the minerals in myrmekite formation of the Types A, B and C.

Type	Type A			Type B				Type C						Ab-rich rim		
Sample	MIU2-34			DH13-15				DH13-8						DH13-8		
No.	M13			M11				M10						M6		
Location	A1	A15	A20	A24	A16	A10	A1	A23	A15	B2	A11	A8	A2	A15	A14	A8
Mineral[*1]	**Pl**	**MP**	**Kfs**	**Pl**	**Ab**	**MP**	**Kfs**	**Pl**	**PML-MP**	**PML-MKfs**	**Ab**	**KML-MP**	**Kfs**	**Pl**	**Ab**	**Kfs**
(wt%)																
SiO_2	65.75	65.64	64.57	64.32	67.08	66.46	64.92	65.05	66.65	64.22	67.68	65.98	64.67	62.15	66.69	65.97
TiO_2	-	-	-	-	-	-	-	-	-	-	-	-	-	-	-	-
Al_2O_3	21.62	20.82	17.96	21.47	20.02	21.03	18.10	21.86	20.78	17.93	20.30	21.56	17.63	23.12	20.15	17.78
FeO	-	-	-	-	-	-	-	-	-	-	-	-	-	-	-	-
MnO	-	-	-	-	-	-	-	-	-	-	-	-	-	-	-	-
MgO	-	-	-	-	-	-	-	-	-	-	-	-	-	-	-	-
CaO	2.52	1.88	0.02	3.20	1.14	2.36	0.00	3.27	1.92	0.01	1.26	2.73	0.02	5.08	1.27	0.02
Na_2O	10.02	10.52	0.32	9.41	11.30	10.61	0.57	9.92	10.58	0.54	11.32	10.10	0.65	8.42	11.12	0.80
K_2O	0.40	0.19	16.78	0.28	0.14	0.07	16.30	0.44	0.13	16.34	0.11	0.18	16.02	0.23	0.15	16.24
Total	100.31	99.05	99.65	98.68	99.68	100.53	99.89	100.54	100.06	99.04	100.67	100.55	98.99	99.01	99.38	100.80
(atom)																
cfu[*2]	8	8	8	8	8	8	8	8	8	8	8	8	8	8	8	8
Si	2.88	2.91	3.00	2.87	2.95	2.90	3.00	2.86	2.92	3.00	2.95	2.88	3.02	2.78	2.94	3.02
Ti	-	-	-	-	-	-	-	-	-	-	-	-	-	-	-	-
Al	1.12	1.09	0.98	1.13	1.04	1.08	0.99	1.13	1.07	0.98	1.04	1.11	0.97	1.22	1.05	0.96
Fe	-	-	-	-	-	-	-	-	-	-	-	-	-	-	-	-
Mn	-	-	-	-	-	-	-	-	-	-	-	-	-	-	-	-
Mg	-	-	-	-	-	-	-	-	-	-	-	-	-	-	-	-
Ca	0.12	0.09	0.00	0.15	0.05	0.11	0.00	0.15	0.09	0.00	0.06	0.13	0.00	0.24	0.06	0.00
Na	0.85	0.90	0.03	0.81	0.96	0.90	0.05	0.84	0.90	0.05	0.96	0.86	0.06	0.73	0.95	0.07
K	0.02	0.01	1.00	0.02	0.01	0.00	0.95	0.02	0.01	0.97	0.01	0.01	0.95	0.01	0.01	0.95
Total	5.00	5.00	5.01	4.98	5.01	4.99	4.99	5.00	4.99	5.00	5.01	4.99	5.00	5.00	5.01	5.00
Ab	85.86	90.00	2.91	82.65	94.12	89.11	5.00	83.17	90.00	4.90	93.20	86.00	5.94	73.98	93.15	6.85
An	12.12	9.00	0.00	15.31	4.90	10.89	0.00	14.85	9.00	0.00	5.83	13.00	0.00	24.67	5.87	0.12
Or	2.02	1.00	97.09	2.04	0.98	0.00	95.00	1.98	1.00	95.10	0.97	1.00	94.06	1.35	0.98	93.03
V[*3]	100.49	100.38	108.62	100.51	100.36	100.31	108.44	100.50	100.38	108.45	100.37	100.41	108.36	100.50	100.37	108.27

[*1] Pl : magmatic plagioclase, MP : myrmekitic plagioclase, Ab : plagioclase in albite-rich layer, PML-MP and PML-MKfs : myrmekitic plagioclase and K-feldspar in the PML (plagioclase-side myrmekite layer), KML-MP: myrmekitic plagioclase in the KML (K-feldspar-side myrmekite layer), and Kfs : magmatic K-feldspar.

[*2] cfu: cation per fomula unit.

[*3] Molar volume (cm^3/mol) for feldspar were calculated by propotion among albite (100.25 cm^3 / mol), anorthite (100.79 cm^3 / mol) and orthoclase (108.87 cm^3 / mol).

This is the peer-reviewed, final accepted version for American Mineralogist, published by the Mineralogical Society of America.
The published version is subject to change. Cite as Authors (Year) Title. American Mineralogist, in press.
DOI: https://doi.org/10.2138/am-2021-7956. http://www.minsocam.org/

Table 2 Mineral assemblage and the volume (areal) relations of reactants and products in the Types A, B and C.

Type	Sample No.	Mineral assemblage			Area (μm^2)						Volume (areal) ratio of product minerals[*2]	Volume reduction (%)
		Reactant	Products[*1]		Entire	Ab	MP	VQ	Kfs	micro pores		
Type A	MIU2-34 M13	Pl, Kfs	Myr	MP, VQ, MKfs	19970	-	18228	1189	62	491	MP : VQ : Kfs = 1 : 0.065 : 0.003	2.52
Type B	DH13-15 M11	Pl, Kfs	Myr	MP, VQ	5074	-	4538	415	-	121	Myr : Ab layer = 1 : 2.414	2.45
			Ab layer	Ab	11982	11953	-	-	-	29	MP : VQ : Ab = 0.916 : 0.084 : 2.414	0.00
Type C	DH13-8 M10	Pl, Kfs	KML	KML-MP KML-VQ	3628	-	3114	352	-	162	KML : Ab layer : PML = 1 : 0.681 : 3.688	4.68
			Ab layer	Ab	2362	2361	-	-	-	1	KML-MP : KML-VQ : Ab : PML-MP : PML-VQ : PML-Kfs = $\frac{0.898 : 0.102}{(1)} : 0.681 : \frac{3.388 : 0.236 : 0.064}{(3.688)}$	0.04
			PML	PML-MP PML-VQ PML-MKfs	12944	-	11741	817	221	165		1.29

[*1] KML: K-feldspar-side myrmekite layer, PML: plagioclase-side myrmekite layer, MP : myrmekitic plagioclase, VQ : vermicular quartz, MKfs : myrmekitic K-feldspar, Ab : plagioclase in albite-rich layer, KML-MP and KML-VQ: myrmekitic plagioclase and vermicular quartz in the KML, and PML-MP, PML-VQ, and PML-MKfs: myrmekitic plagioclase, vermicular quartz, and myrmekitic K-feldspar in the PML.

[*2] The volume fraction of product minerals in the plagioclase alteration was estimated from the areal fraction of them by simply assuming the equivalence of areal and volume fractions. The area of product minerals in the myrmekite are identified by BSE images, and the areal ratio was calculated by image processing software (Adobe Photoshop).

This is the peer-reviewed, final accepted version for American Mineralogist, published by the Mineralogical Society of America.
The published version is subject to change. Cite as Authors (Year) Title. American Mineralogist, in press.
DOI: https://doi.org/10.2138/am-2021-7956. http://www.minsocam.org/

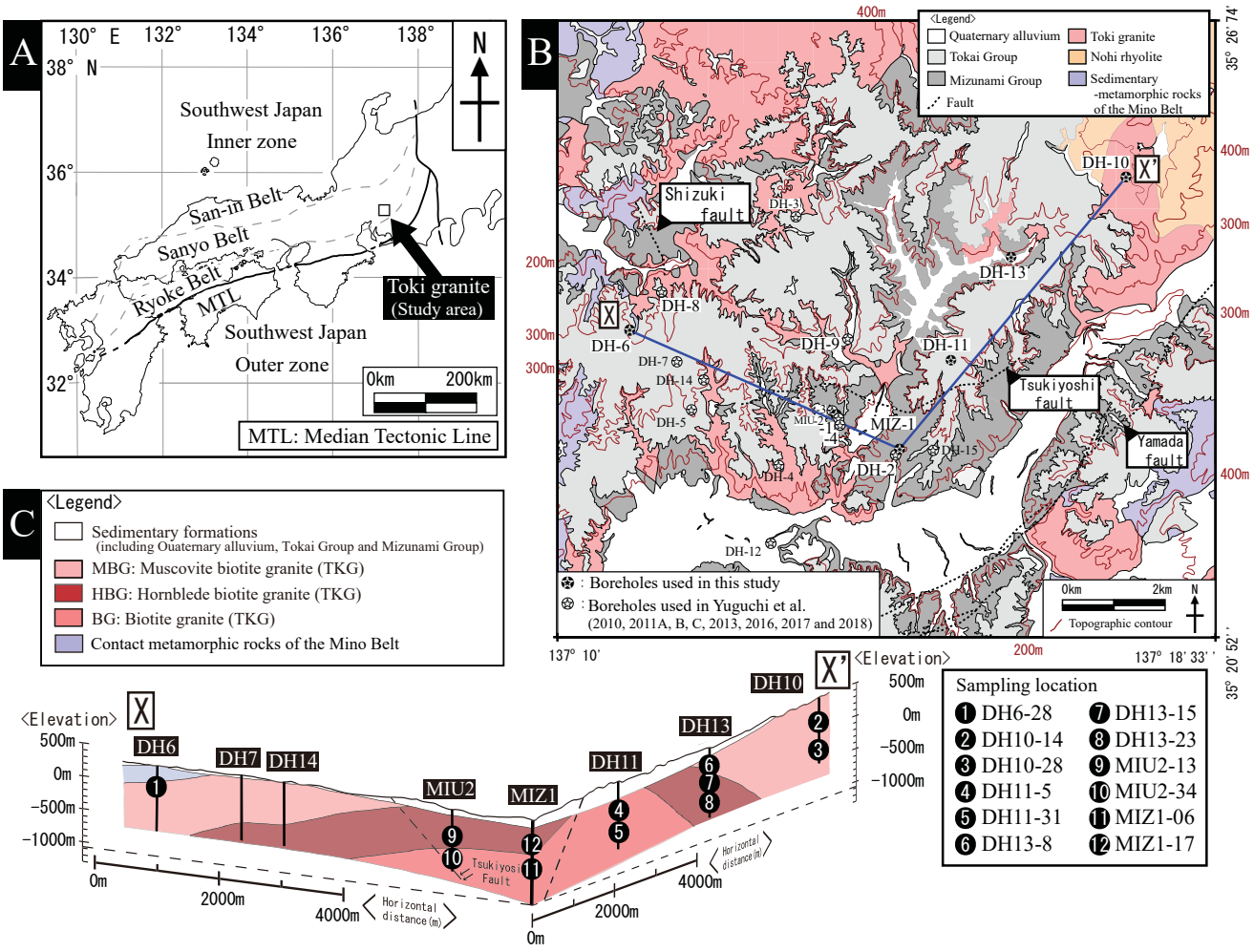

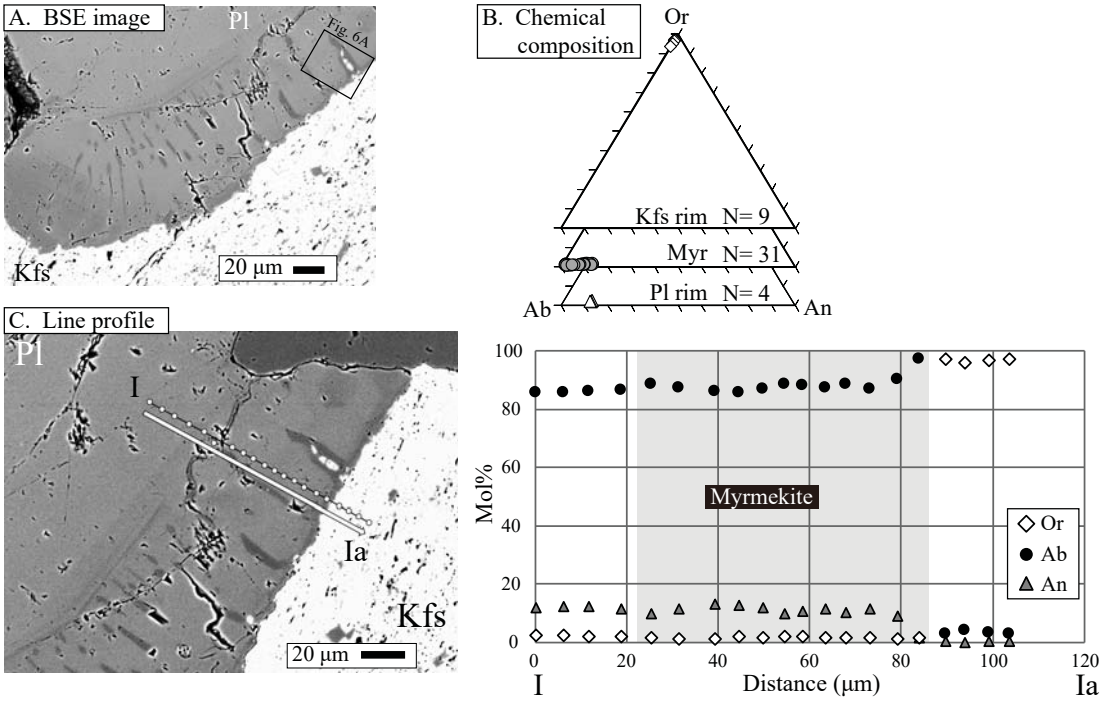

This is the peer-reviewed, final accepted version for American Mineralogist, published by the Mineralogical Society of America.
The published version is subject to change. Cite as Authors (Year) Title. American Mineralogist, in press.
DOI: https://doi.org/10.2138/am-2021-7956. http://www.minsocam.org/

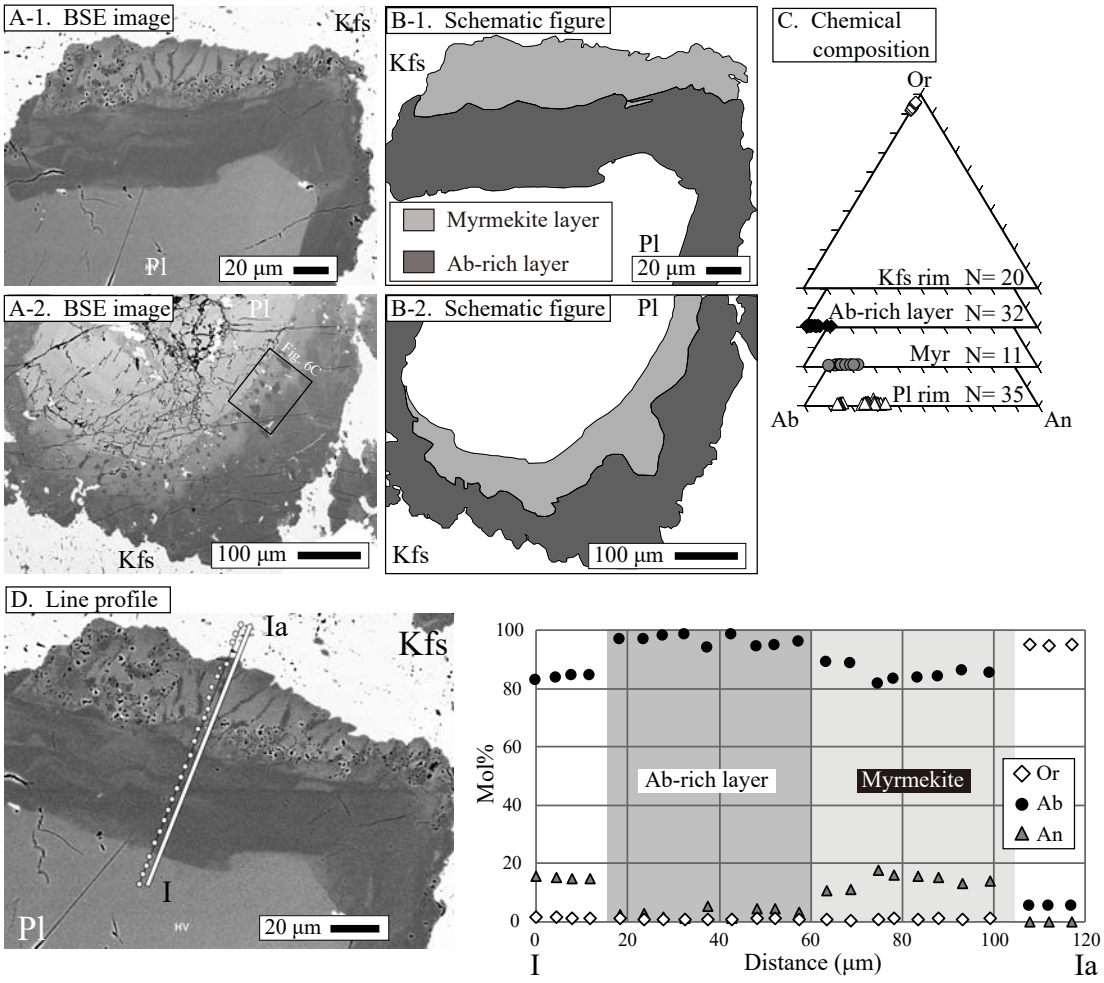

This is the peer-reviewed, final accepted version for American Mineralogist, published by the Mineralogical Society of America.
The published version is subject to change. Cite as Authors (Year) Title. American Mineralogist, in press.
DOI: https://doi.org/10.2138/am-2021-7956. http://www.minsocam.org/

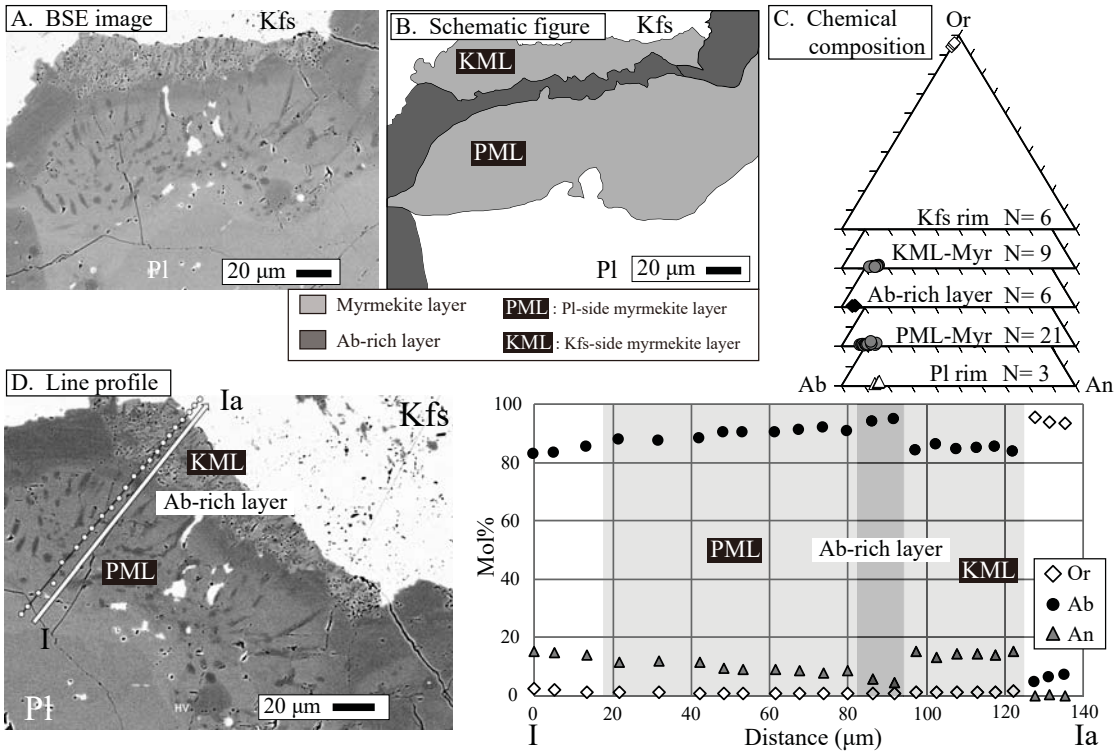

This is the peer-reviewed, final accepted version for American Mineralogist, published by the Mineralogical Society of America.
The published version is subject to change. Cite as Authors (Year) Title. American Mineralogist, in press.
DOI: https://doi.org/10.2138/am-2021-7956. http://www.minsocam.org/

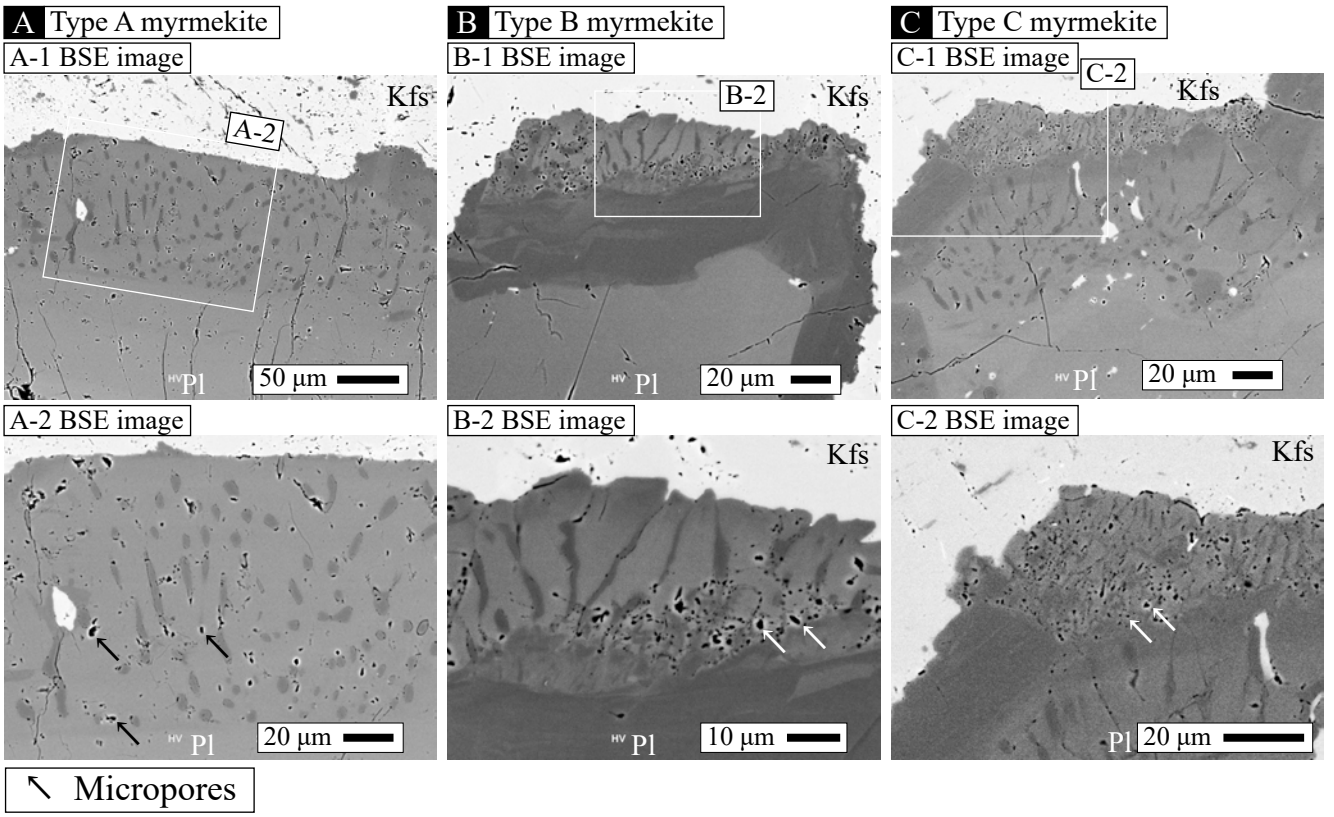

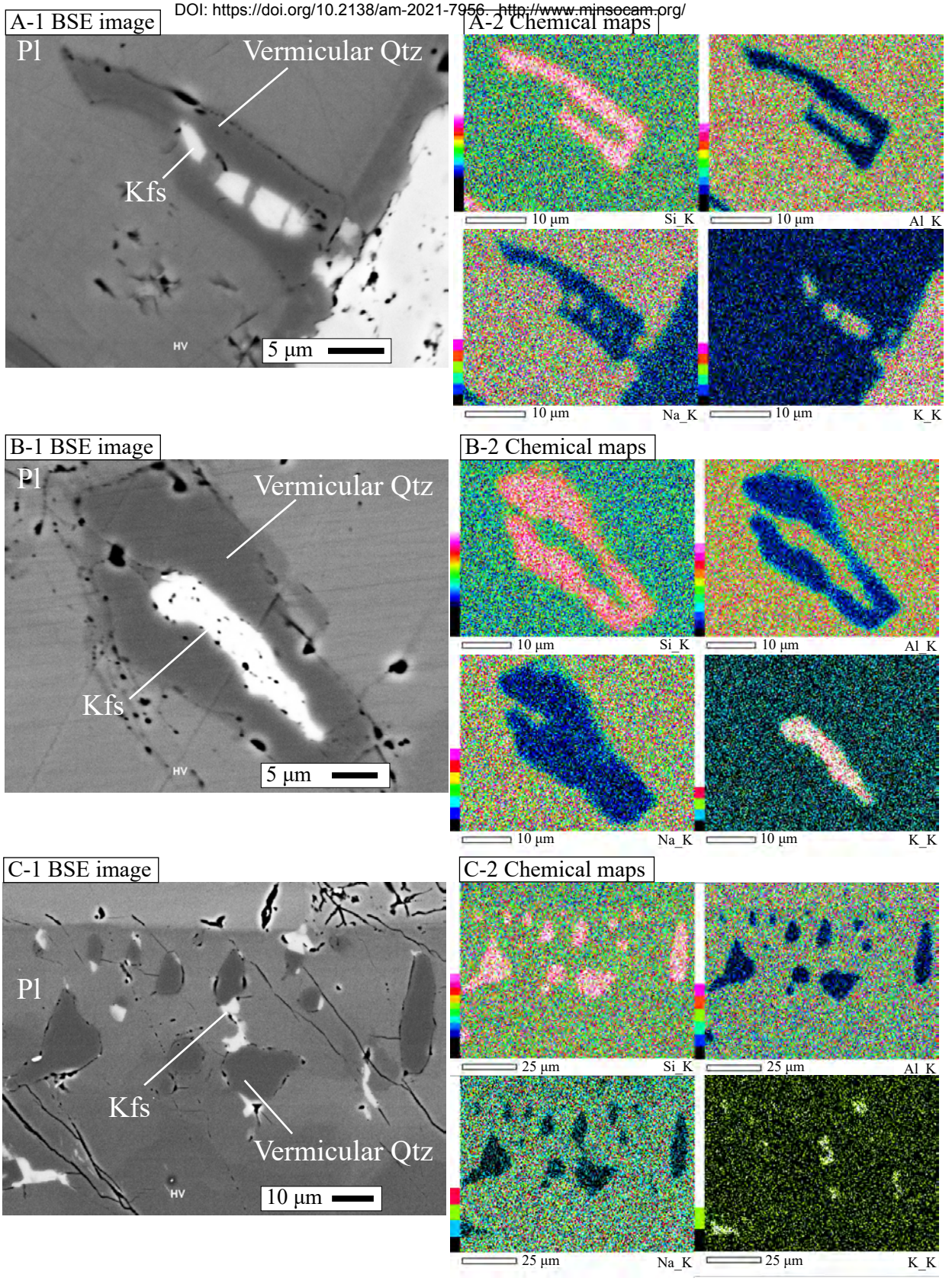

This is the peer-reviewed, final accepted version for American Mineralogist, published by the Mineralogical Society of America.
The published version is subject to change. Cite as Authors (Year) Title. American Mineralogist, in press.
DOI: https://doi.org/10.2138/am-2021-7956. http://www.minsocam.org/